Globally Convergent Adaptive Tracking of Spacecraft Angular Velocity with Inertia Identification

Amit K. Sanyal, Madhusudhan Chellappa, Jean Luc Valk, Jinglai Shen
Jasim Ahmed and Dennis S. Bernstein *

Department of Aerospace Engineering,
The University of Michigan
Ann Arbor, Michigan 48109-2118
(734) 764-3719, FAX (734) 763-0578
dsbaero@engin.umich.edu

March 8, 2003

Abstract

The problem of a rigid body tracking a desired angular velocity trajectory is addressed using adaptive feedback control. An adaptive controller is developed for a planar rotating body tracking a desired angular velocity command. Lyapunov analysis is used to show that tracking is achieved globally. A periodic angular velocity command is then used to identify the inertia parameter. The adaptive controller is implemented on a triaxial attitude control testbed with fan thrusters. A lack of convergence of the inertia estimate indicates the presence of an input nonlinearity. To account for this effect, a piecewise linear approximation of this nonlinearity is inverted to obtain improved angular velocity tracking and inertia identification. Finally, to eliminate residual tracking error, an adaptive algorithm is used for improved feedback linearization. Lyapunov analysis is used to show convergence of the angular velocity and inertia estimate errors. The approach is validated by experimental implementation.

*Research supported in part by the Air Force Office of Scientific Research under Grant F49620-98-1-0037.

1 Introduction

Stabilization of a single free rigid body in three dimensions is a widely studied and fundamental problem in spacecraft dynamics. Although the problem is trivial in the presence of three control torques, significant research has been devoted to the cases of two torques [1] - [5] and one torque [2], [3], [6]. If minimum fuel or minimum time performance is required in addition to stabilization, then this problem is challenging even in the case of three torque inputs [7], [8]. If rotors are used to provide control torques, then the problem involves multiple bodies and significantly greater complexity [9], [10].

The above remarks are based on the assumption that the spacecraft mass distribution is known and constant. However, in practice there are limitations due to fuel usage, moving appendages, and complex geometry on the ability to determine the mass distribution. Hence it is of interest to determine stabilizing controllers that can operate with as little inertia information as possible.

In the present paper we address the inertia-uncertainty problem by deriving an adaptive controller that tracks an angular velocity command without any information concerning the mass distribution. In addition, the controller we present provides asymptotic tracking of arbitrary angular velocity commands. For a rotating spacecraft modeled as a rigid body, this controller is effectively a PI control law involving 6 integrators. The integrator states, which correspond to the entries of the inertia matrix, converge to the actual spacecraft inertia under sufficiently persistent excitation.

It is important to point out that angular velocity tracking does not provide a guarantee of inertial spacecraft attitude control. The inclusion of attitude states within an inertia-independent adaptive controller is given in [11]. The tracking problem considered in the present paper can be viewed as an extension of [11] to the case in which attitude measurements are not available.

The contents of the paper are as follows. In Section 2 we present an adaptive control scheme that provides angular velocity tracking for a planar rigid body with unknown inertia. In addition, we present a method to identify the unknown inertia, and apply the method to a numerical example. A description of the testbed and control hardware used for experiments is presented in Section 3. In Section 4 we present experimental results obtained for single-degree-of-freedom rotation. The lack of convergence of inertia estimate indicates the presence of an input nonlinearity. To account for this effect, a piecewise linear approximation of this nonlinearity is inverted to obtain improved angular velocity tracking and inertia identification. Finally, to eliminate residual tracking error, an adaptive algorithm is used for improved feedback linearization. Lyapunov analysis is used to show convergence of the angular velocity and inertia estimate errors. The approach is validated by

experimental implementation.

2 Adaptive Control of a Planar Rotating Body

Consider a rigid body constrained to rotate about a fixed axis passing through its center of mass. For $t \geq 0$, the equation of motion is given by

$$\dot{\omega} = \frac{1}{J}\tau, \tag{1}$$

where ω is the angular velocity of the body about its rotation axis, J is the moment of inertia of the body about its rotation axis, and τ is the applied torque. We assume that J is unknown.

Let $\nu : [0, \infty) \to \mathcal{R}$ denote the desired angular velocity of the body. We assume that ν is C^1. Defining the angular velocity error $\tilde{\omega}$ by $\tilde{\omega} \triangleq \omega - \nu$, it follows from (1) that $\tilde{\omega}$ satisfies

$$\dot{\tilde{\omega}} = -\dot{\nu} + \frac{1}{J}\tau. \tag{2}$$

The control objective is to determine τ such that $\tilde{\omega} \to 0$ as $t \to \infty$ for all initial conditions $\omega(0)$ and without knowledge of J. The following result provides an adaptive controller for angular velocity tracking based on an estimate $\hat{J}(t)$ of J.

Theorem 1. Assume that $\dot{\nu}$ is bounded, let $k > 0$ and $q > 0$, and consider the closed-loop system consisting of (2) and the adaptation control law

$$\dot{\hat{J}} = -q\dot{\nu}\tilde{\omega}, \tag{3}$$

$$\tau = -k\tilde{\omega} + \dot{\nu}\hat{J}. \tag{4}$$

Then $\tilde{\omega} \to 0$ as $t \to \infty$ for all $\omega(0)$ and $\hat{J}(0)$. Furthermore, $\hat{J}$ is bounded for all $t \geq 0$, and $\dot{\hat{J}} \to 0$ as $t \to \infty$.

Proof. Define the error $\tilde{\mathcal{J}}$ in the inertia estimate by $\tilde{J} \triangleq \hat{J} - J$. Using (2) and (3), we obtain the linear time-varying system

$$\dot{\tilde{\omega}} \triangleq -\frac{k}{J}\tilde{\omega} + \frac{\dot{\nu}}{J}\tilde{J}, \tag{5}$$

$$\dot{\tilde{J}} = -q\dot{\nu}\tilde{\omega}. \tag{6}$$

Note that $[\tilde{\omega}\ \tilde{J}] = [0\ 0]$ is an equilibrium of (5), (6).

To prove asymptotic tracking, consider the positive-definite Lyapunov candidate

$$V(\tilde{\omega}, \tilde{J}) = \frac{1}{2}\left(J\tilde{\omega}^2 + \frac{1}{q}\tilde{J}^2\right), \tag{7}$$

which does not depend explicitly on time and is radially unbounded. The time derivative of V along the trajectories of the closed-loop system is given by

$$\dot{V}(\tilde{\omega}, \tilde{J}) = -k\tilde{\omega}^2 + \dot{\nu}\tilde{J}\tilde{\omega} + \frac{1}{q}\tilde{J}\dot{\tilde{J}} = -k\tilde{\omega}^2, \tag{8}$$

which shows that $\dot{V}$ is negative semi-definite and is not an explicit function of time. Hence $V(\tilde{\omega}(t), \tilde{J}(t)) \leq V(\tilde{\omega}(0), \tilde{J}(0))$ for all $t \geq 0$, and, since V is radially unbounded, it follows that $\tilde{\omega}$ and $\tilde{J}$, and hence $\hat{J}$ are bounded.

Next, to show that $\tilde{\omega} \to 0$ as $t \to \infty$, note that the time derivative of $\dot{V}$ along the trajectories of the system is given by

$$\ddot{V}(\tilde{\omega}, \tilde{J}, t) = \frac{2k\tilde{\omega}}{J}(k\tilde{\omega} - \dot{\nu}(t)\tilde{J}). \tag{9}$$

Since $\tilde{\omega}$, $\tilde{J}$ and $\dot{\nu}$ are bounded and J is constant, it follows that $\ddot{V}(\tilde{\omega}(t), \tilde{J}(t), t)$ is bounded for all $t \geq 0$. It now follows from Theorem 5.4 of [12] that $\tilde{\omega} \to 0$ as $t \to \infty$. Since $\tilde{\omega} \to 0$ as $t \to \infty$ and $\dot{\nu}$ is bounded, it follows from (6) that $\dot{\tilde{J}} \to 0$ and thus $\dot{\hat{J}} \to 0$ as $t \to \infty$. □

Note that the control law given by (3) does not require knowledge of the inertia J of the body. Although $\dot{\hat{J}}$ converges to zero, $\hat{J}$ does not necessarily converge, and, if it does converge, it does not necessarily converge to the actual inertia J. The following result gives a sufficient condition under which $\hat{J}$ converges to J.

Proposition 1. Assume that ν is not constant and periodic. Then, under the control and adaptation law given by (3) and (4), $\hat{J} \to J$ as $t \to \infty$.

Proof. Consider the Lyapunov candidate V defined by (7) so that $\dot{V}$ is given by (8), and define $E \triangleq \dot{V}^{-1}(0) = \{[\tilde{\omega}\ \tilde{J}] : \tilde{\omega} = 0\}$. Let $\mathcal{M}$ be the largest invariant set in E, and let $[\tilde{\omega}\ \tilde{J}]$ be a trajectory in $\mathcal{M}$. Then $\tilde{\omega} \equiv 0$ and $\dot{\tilde{\omega}} \equiv 0$. Now (6) implies that $\dot{\tilde{J}} \equiv 0$, and (5) implies that $\dot{\nu}(t)\tilde{J} \equiv 0$. Hence $\tilde{J}$ is constant and, since $\nu(t)$ is not constant, it follows that $\tilde{J} \equiv 0$. Consequently, $\mathcal{M} = \{(0, 0)\}$. Since $\nu(t)$ is periodic, it now follows from Theorem 2.8 of [13] (p. 58) that $[\tilde{\omega}\ \tilde{J}] \to \mathcal{M}$ as $t \to \infty$, and thus $\tilde{J} \to 0$, or $\hat{J} \to J$, as $t \to \infty$. □

Proposition 2. Assume that $\dot{\nu}$ is periodic, and assume there exist $\alpha > 0$ and $T > 0$ such that, for all $t > 0$,

$$\int_t^{t+T} \dot{\nu}^2(s)ds \geq \alpha. \tag{10}$$

Then, under the control and adaptation law (3) and (4), $\tilde{J} \to 0$ as $t \to \infty$ exponentially.

Proof. Since ν is C^1, $\dot{\nu}$ is continuous and periodic, and hence bounded. The result now follows from Corollary 4.3.1 of [14]. □

To illustrate Theorem 1 and Proposition 1, consider the sinusoidal angular velocity command

$$\nu(t) = \frac{a}{\omega_0}(1 - \cos(\omega_0 t)),$$

where $a = 1.2$ rad^2/sec^2 and $\omega_0 = 1.0$ rad/sec. The inertia of the planar rotating body is taken to be $J = 1.0$ kg-m^2/rad^2, and its initial estimate is $\hat{J}(0) = 0.7$ kg-m^2/rad^2. The gains are $k = 4.8$ kg-m^2/rad^2-sec and $q = 2.8$ kg-m^2-sec^2/rad^4. The initial angular velocity error is given by $\tilde{\omega}(0) = 0.35$ rad/s. The angular velocity tracking error, inertia estimate error, and applied input torque are shown in Figure 1. It can be seen that $\tilde{\omega}$ converges to zero and $\hat{J}$ converges to J within 15 seconds. The torque is seen to have an initial transient with $\tau(0) = -k\tilde{\omega}(0) + \dot{\nu}(0)\hat{J}(0) = -1.68$ N-m/rad, where $\dot{\nu}(0) = 0$ rad/sec^2.

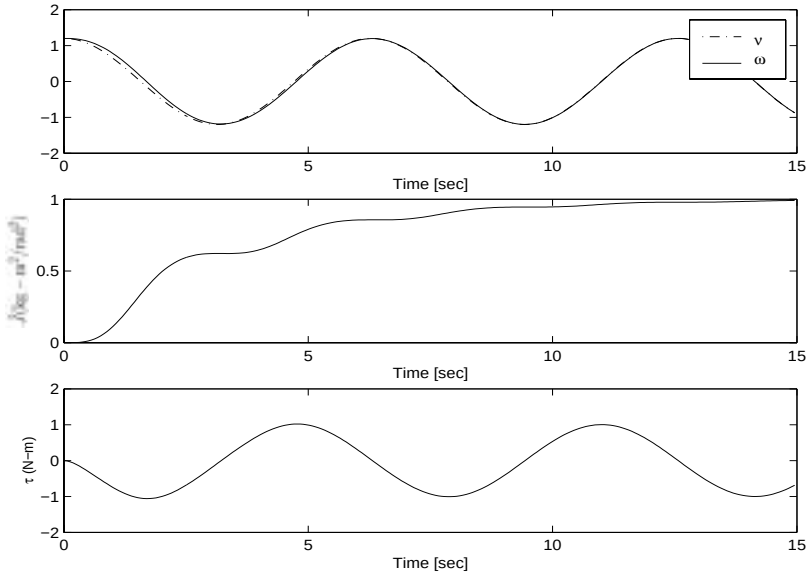

Figure 1: Angular Velocities, Inertia Estimate and Control Torque for the Planar Rotating Body Tracking a Sinusoidal Angular Velocity Command

Next, to see how the adaptive controller of Theorem 1 performs on a command signal that is not differentiable, consider the triangle wave angular velocity command

$$\nu(t) = \begin{cases} t - 2\lfloor t/2 \rfloor, & \text{if } 2n \le t < 2n+1, \\ 2 - t + 2\lfloor t/2 \rfloor, & \text{if } 2n+1 < t \le 2n+2, \end{cases}$$

where n is a nonnegative integer. The initial conditions and gains are the same as in the previous example. The angular velocity tracking error, inertia estimate error, and applied input torque are

shown in Figure 2. This figure shows that the adaptive controller (3) and (4) is effective even when the angular velocity signal is not C^1.

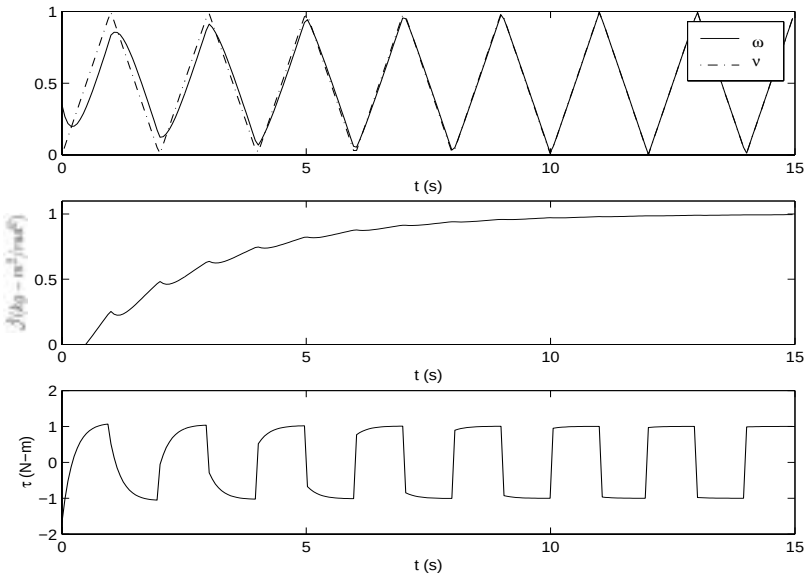

Figure 2: Angular Velocities, Inertia Estimate and Control Torque for the Planar Rotating Body Tracking a Triangle Angular Velocity Command

3 Triaxial Attitude Control Testbed

3.1 Mechanical Setup

The testbed used for experiments in this paper is based on a spherical air bearing manufactured by Space Electronics, Inc., Berlin, CT. The aluminum sphere of diameter 11 inch floats on a thin film of air that exits holes located in the surface of the cup. Air at 70 psi is supplied to the cup by means of a hose that passes through the center of the vertical support.

A one-piece 32 inch stainless steel shaft passes through the center of the sphere and extends between a pair of 24-inch circular mounting plates. This shaft is designed to withstand stresses that might otherwise distort the sphere. All mounting plates are made from 1/4-inch aluminum alloy with 1/4-20 holes tapped in a 1 inch grid. The 14-inch aluminum extension shafts connect the circular mounting plates to the 30-inch $\times$ 30-inch square mounting plates. The distance between the square plates is thus 5 feet. All shafts have hollow interior to allow wiring through the sphere and between any two points. Access holes of size 1 inch $\times$ 2 inch are cut into the plates and shafts to allow cable jacks and plugs to be passed between connection points. The total weight of the levitated components described thus far is 180 lb. At 70 psi air pressure, the air bearing can support an additional 180 lb of components.

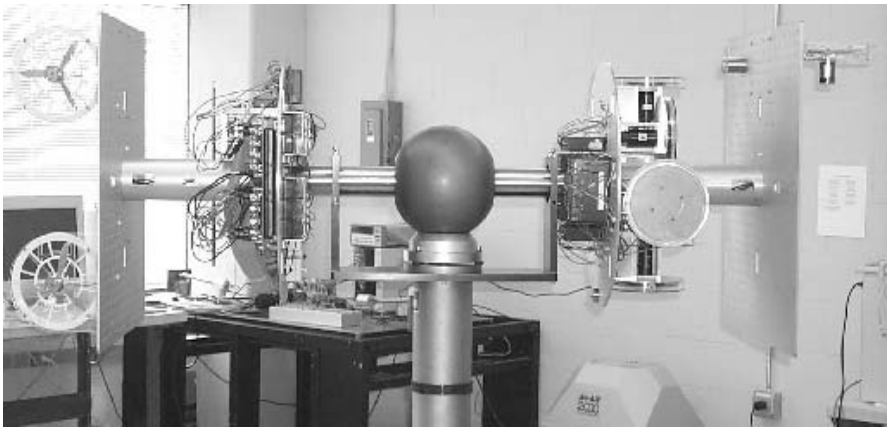

Figure 3: Triaxial Air Bearing Testbed. This testbed, which is based on a spherical air bearing, allows low friction, three-dimensional motion with unrestricted roll and yaw and $\pm 45^\circ$ pitch.

The spherical air bearing allows unrestricted motion in yaw (motion about the vertical axis) and roll (motion about the longitudinal shaft axis). The plates and shafts are designed to allow $\pm 45^\circ$ pitch (motion about a horizontal axis) at all roll and yaw angles.

Once the main components are mounted, additional masses can be added to modify the final mass distribution. For 1-dimensional experiments, the center of mass is located in the vertical line that passes through the rotational center. When the center of mass is not located at the rotational center, this mass distribution balances pitch motion, provides pendulum dynamics in roll, and yields predominantly yaw dynamics for the 1-dimensional experiments. For 3-dimensional experiments, the center of mass can be located at the rotational center to balance the system in both roll and pitch.

3.2 Control Hardware

For attitude control experiments, the triaxial attitude control testbed uses on-board sensors. A three-axis magnetometer determines the direction of the Earth's magnetic north; a three-axis accelerometer measures gravitational and centripetal acceleration; and a three-axis gyro measures angular velocity. For the present paper only the gyros are needed.

The three-axis gyro is comprised of three Gyrochip Horizon rate sensors manufactured by Systron Donner, Concord, CA. The input range of these sensors is ± 90 deg/sec and, according to specifications, their bandwidth is greater than 18 Hz. Under static conditions, that is, $\omega = 0$, we measured the rms gyro noise to be about 1.3 mV, which corresponds to .06 deg/sec. Since the gyro measurement range is 0 V to 5 V, the sensor dynamic range is found to be 71.7 dB, or 12 analog-digital conversion bits. Operation of fan thrusters does not affect the gyro noise significantly.

For real-time on-board processing, we use an embedded processor developed by Quanser Consulting. This processor is based on a 586 processor with 4 GByte solid state hard disk and Multi-Q I/O boards allowing up to 24 A/D channels, 24 D/A channels, and 16 encoder channels. The A/D and D/A channels have a resolution of 13 bits over a ± 5 V range. The A/D sampling occurs sequentially with an acquisition time of 20 μsec per channel, while the D/A conversion also occurs sequentially with a latency of 5 μsec per channel. The operating system is based on the Quanser Consulting WinCon real-time controller, which is compatible with the MathWorks Real-Time Workshop for implementing controllers programmed in Simulink. Communication with the host PC for experiment monitoring, parameter modification, and data acquisition is accomplished through a wireless ethernet connection.

For control actuation the triaxial attitude control testbed uses six reaction wheels and propeller thrusters. Each reaction wheel actuator is based on a 100 W brushless DC motor manufactured by Maxon (model 118896). This motor allows 2.8 A max continuous current at 5000 rpm, 729 mN-m stall torque, and 38.2 mN-m/A torque constant. Mounted on the shaft of each motor is a 1/8-inch thick steel disk of radius 7 inch. Maximum measured spin rate is 8500 rpm. Each motor is driven by a brushless (current-regulated) PWM amplifier manufactured by Copley (Model 5121V). This trapezoidally commutated amplifier is capable of 10 A continuous and 20 A peak. Electric power for a pair of motors and a pair of amplifiers is provided at 36 V by three 12-V lead acid batteries each rated at 1.3 A-hr. A total of six reaction wheels and six amplifiers have been mounted on the triaxial air bearing to provide a pair of reaction wheels for each axis. The amplifiers are operated in current mode to provide commandable torque to the wheels.

While each motor is equipped with a 500-line encoder giving a resolution of $360^\circ/2000$, the wheel angle is used only for modeling and diagnostic purposes. For experiments, we use the frequency converter feature of the Model 5121 amplifier to obtain a synthesized tachometer signal from each motor's Hall sensor. This allows us to monitor each motor's spin rate and stored angular momentum.

The experiments described here use the four propeller thrusters. These thrusters are based on the same Maxon motors and Copley amplifiers used by the reaction wheels without encoders. Without the encoders mounted, these motors have a dual protruding shaft to which a pair of propellers is mounted to obtain direction-symmetric thrust. Unlike the reaction wheels, however, the Copley amplifiers for the thrusters are operated in velocity mode to provide a commandable torque.

4 Experimental Results

4.1 Preliminary Analysis

The adaptive control algorithm described in Section 2 was tested on the triaxial attitude control testbed. In this section, we detail our experimental results and touch upon some practical implementation issues. As already mentioned we consider only yaw motion of the testbed with thrusters used for actuation.

First, we have

$$\omega = K_{\text{gyro}} V_{\text{gyro}}, \qquad \tau = K_{\text{fan}} V_{\text{fan}}, \tag{11}$$

where V_{gyro} is the voltage output of the gyro, K_{gyro} is the conversion coefficient from V_{gyro} in volts to ω in deg/sec, V_{fan} is the voltage input to the thruster amplifiers, and K_{fan} is the conversion coefficient from V_{fan} in volts to the control torque τ in N-m. From equation (1) we see that $\dot{V}_{\text{gyro}} = V_{\text{fan}}/J'$, where the scaled inertia $J' \triangleq JK_{\text{gyro}}/K_{\text{fan}}$. Note that the units of J' are sec. We define $V_{\text{ref}} \triangleq \nu/K_{\text{gyro}}$ and $\tilde{V} \triangleq V_{\text{gyro}} - V_{\text{ref}}$. We can thus rewrite (3) as

$$V_{\text{fan}} = -k'\tilde{V} + \dot{V}_{\text{ref}}\hat{J}', \tag{12}$$

where $k' \triangleq kK_{\text{gyro}}K_{\text{fan}}$ and $\hat{J}'$ is the estimate of J'. The adaptive law (4 can be written as

$$\dot{\hat{J}}' = -q'\dot{V}_{\text{ref}}\tilde{V}, \tag{13}$$

where $q' \triangleq qK_{\text{gyro}}^3/K_{\text{fan}}$. Comparing (4) and (5) with (12) and (13), it follows that the conversion coefficients are incorporated within the constants q' and k'. It can be seen that k' is dimensionless and q' has units of V/sec^2. Hence, we can apply the adaptive control algorithm of Section 2 without further calibration. However, to relate our results to physical motion, we calibrated the gyro voltage and found $K_{\text{gyro}} = 45.5$ deg/V-sec. For the remainder of this section we view V_{fan} as the control signal.

4.2 Control Experiments

When ν is constant, the adaptive controller specializes to the proportional controller

$$V_{\text{fan}} = -k'\tilde{V}. \tag{14}$$

Since the plant (1) is an integrator, the closed-loop system with the proportional controller (14) yields zero steady-state error for step commands.

The angular velocity $\omega(t)$ for the sinusoidal command $\nu(t) = 10\sin .2t$ and a proportional gain of k'= 20 sec/V^2 is shown in Figure 4. The angular velocity $\omega(t)$ converges to a periodic signal with

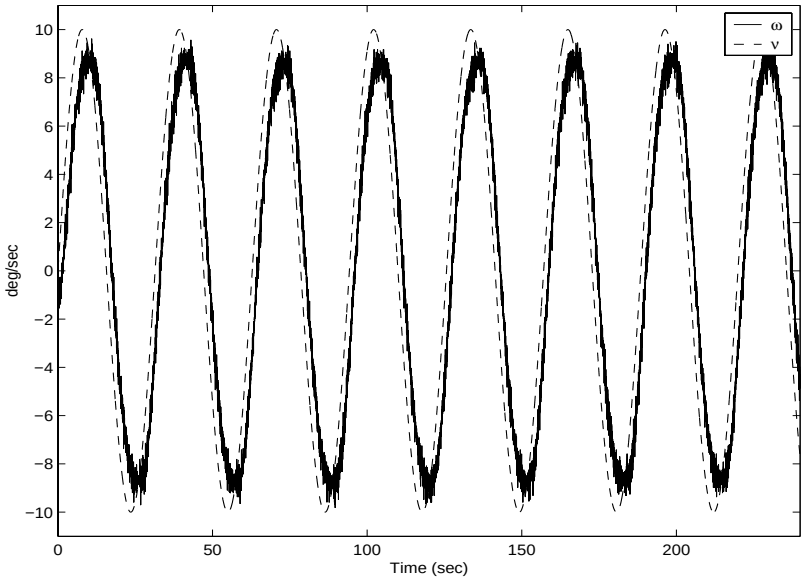

Figure 4: Angular Velocities $\omega(t)$ and $\nu(t)$ Using the Proportional Controller for $\nu(t) = 10\sin .2t$ deg/sec

rms value of about 2.6 deg/sec.

Now we use the adaptive controller for the same command $\nu(t) = 10\sin .2t$ deg/sec. Figure 5 shows $\omega(t)$ and $\nu(t)$ for $k' = 3$, $q' = 1000$ sec/V^2, and initial scaled inertia estimate $\hat{J}'(0) = 0$ sec. The angular velocity error $\tilde{\omega}(t)$ shown in Figure 6 converges to a periodic signal with rms value of about .25 deg/sec and mean value of 0.0061 deg/sec. Figure 7 gives the scaled inertia estimates obtained with $\hat{J}'(0) = 100$ sec and $\hat{J}'(0) = 0$ sec. The scaled inertia estimate converges to a periodic signal with mean value about 37.9 sec and a peak-to-peak amplitude of about 4.5 sec. Simulations and experiments (not shown) indicate that the value of the inertia estimate varies with the frequency of the command signal.

4.3 Actuator Nonlinearity

The oscillation of $\hat{J}'$ suggests the possible presence of an actuator nonlinearity. We therefore plotted $\dot{V}_{\text{gyro}}$ V/sec (obtained by numerically differentiating the measured V_{gyro}) versus V_{fan} V as computed by the adaptive algorithm during an experiment. From this plot, shown in Figure 8, we find that $\dot{V}_{\text{gyro}}$ is a nonlinear function of the computed moment V_{fan}, that is,

$$\dot{V}_{\text{gyro}} = \mathcal{N}(V_{\text{fan}}). \tag{15}$$

The data was fit by the cubic polynomial

$$\mathcal{N}(x) = 0.1677x^3 + 0.0117x^2 + 0.6747x + 0.0078, \tag{16}$$

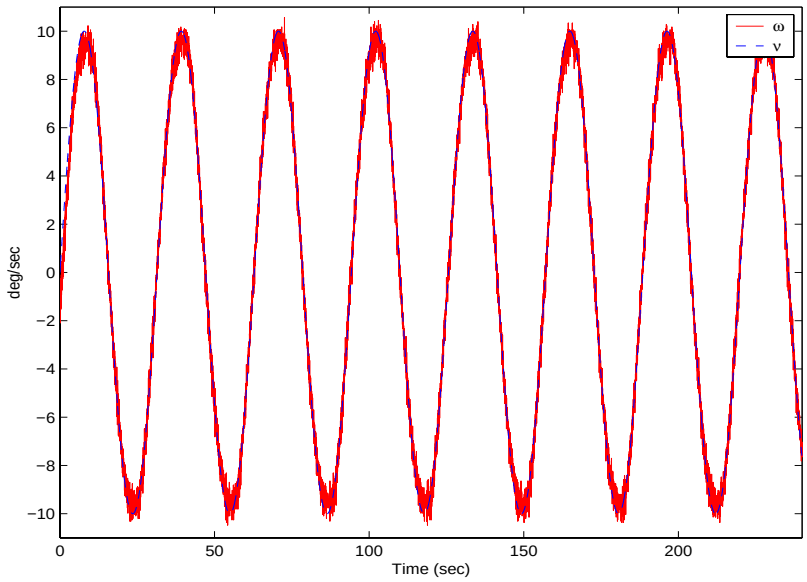

Figure 5: Angular Velocities $\omega(t)$ and $\nu(t)$ Using the Adaptive Controller for $\nu = 10 \sin .2t$ deg/sec

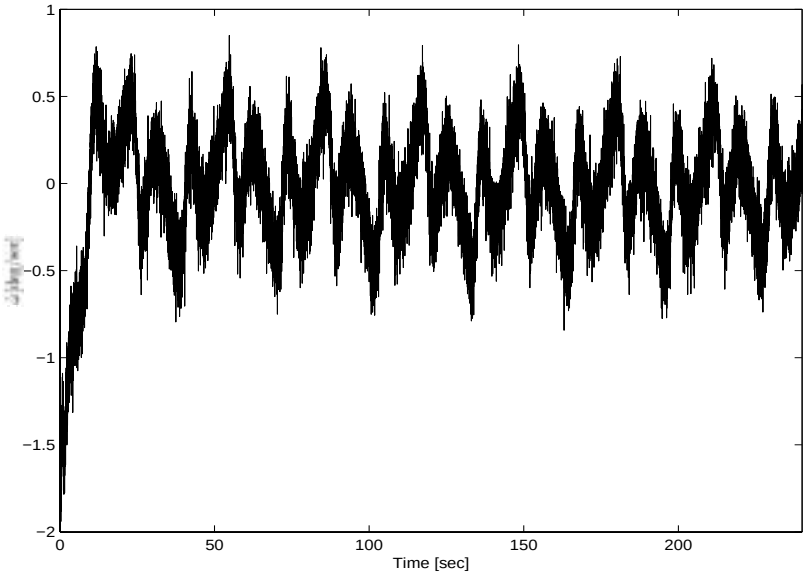

Figure 6: Angular Velocity Tracking Error Using the Adaptive Controller for $\nu(t) = 10 \sin .2t$ deg/sec

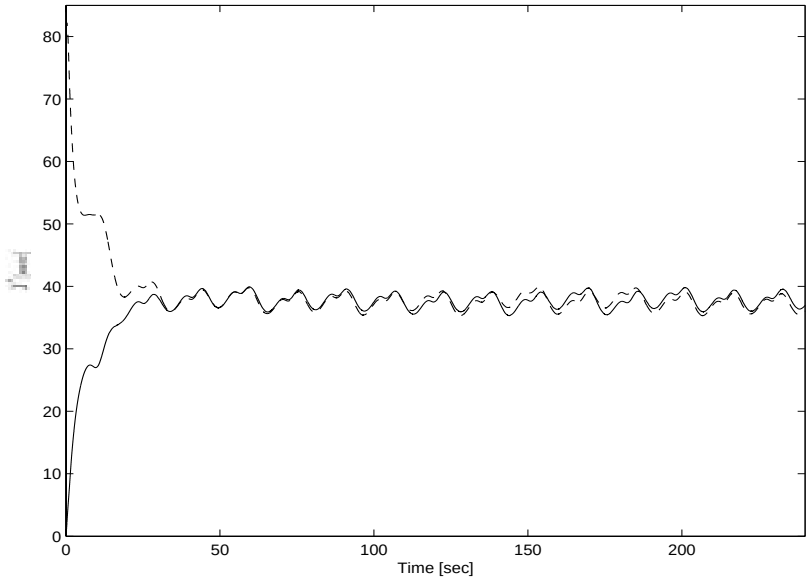

Figure 7: Scaled Inertia Estimate Using the Adaptive Controller for $\nu(t) = 10\sin .2t$ deg/sec, $\hat{J}(0) = 0$ sec, and $\hat{J}(0) = 100$ sec

as shown in Figure 8. From (15), (4), (11), we have

$$\dot{\omega} = K_{\text{gyro}}\mathcal{N}\left(\frac{k\tilde{\omega} + \dot{\nu}\hat{J}}{K_{\text{fan}}}\right). \tag{17}$$

Hence, from (1) the moment input is given by

$$\tau = JK_{\text{gyro}}\,\mathcal{N}\left(\frac{k\tilde{\omega} + \dot{\nu}\hat{J}}{K_{\text{fan}}}\right). \tag{18}$$

To check whether the nonlinearity (16) could cause the oscillations shown in Figure 7, the cubic nonlinearity (16) is included in a simulation of the adaptive closed-loop system for the command $\nu(t) = 10\sin .2t$ deg/sec. From Figures 9 and 10 it is seen that this nonlinearity could indeed cause oscillations similar to those observed from the testbed. The angular velocity error $\tilde{\omega}$, shown in Figure 9, converges to a periodic signal with rms value of about .14 deg/sec and mean value of 0.0066 deg/sec. The scaled inertia estimate converges to a periodic signal with value of about 39 sec and a peak-to-peak amplitude of about 3 sec.

Noting the difficulty involved in inverting the cubic, we obtain a piecewise linear approximation of the cubic nonlinearity, and invert this piecewise linear function. The cubic nonlinearity and the inverse of the piecewise linear approximation are shown in Figure 11.

The simulated response of the closed-loop system is shown in Figures 12 and 13. From these plots it can be seen that the inverse function approximately linearizes the nonlinearity and reduces

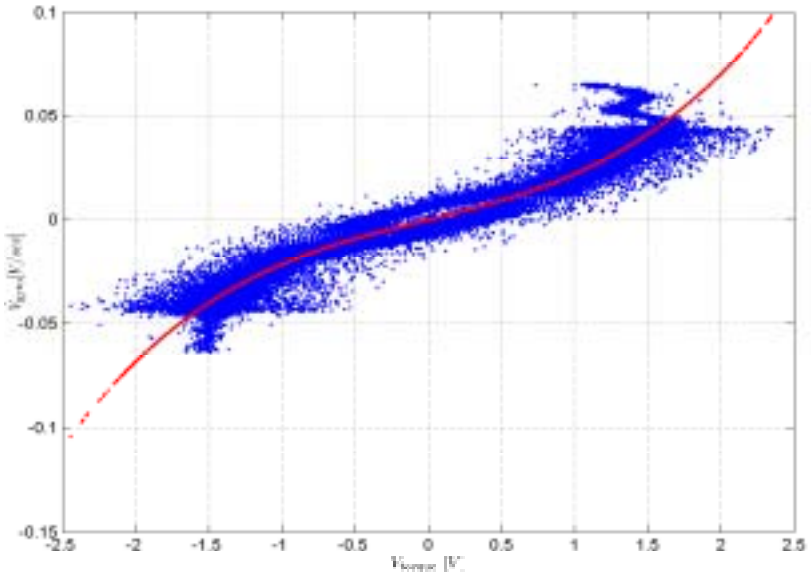

Figure 8: $\dot{V}_{\text{gyro}}$ vs. V_{fan} for $\nu(t) = 10 \sin .1t$ deg/sec

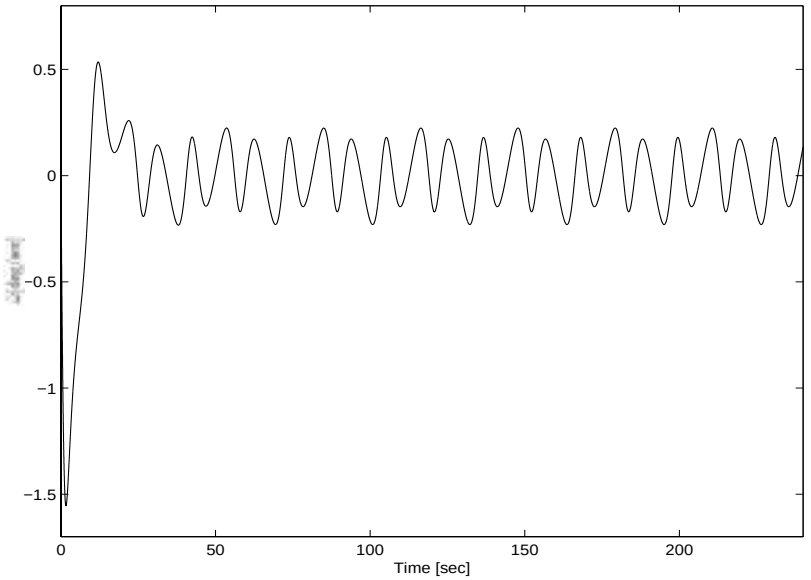

Figure 9: Simulated Angular Velocity Error with Actuator Nonlinearity

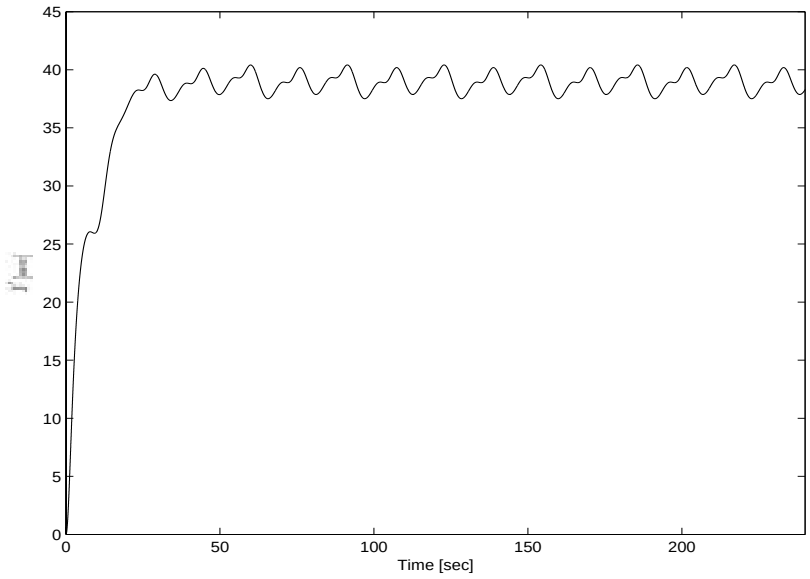

Figure 10: Simulated Scaled Inertia Estimate with Actuator Nonlinearity

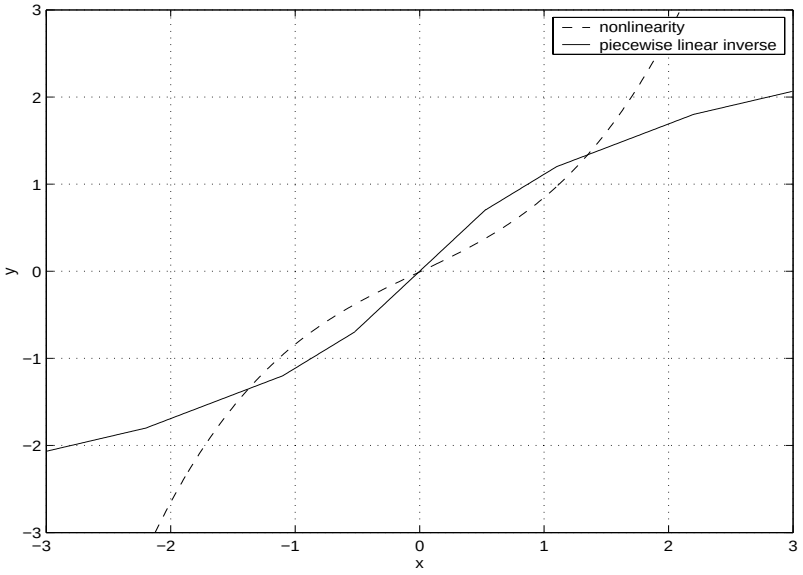

Figure 11: Cubic Actuator Nonlinearity and an Approximate Piecewise Linear Inverse

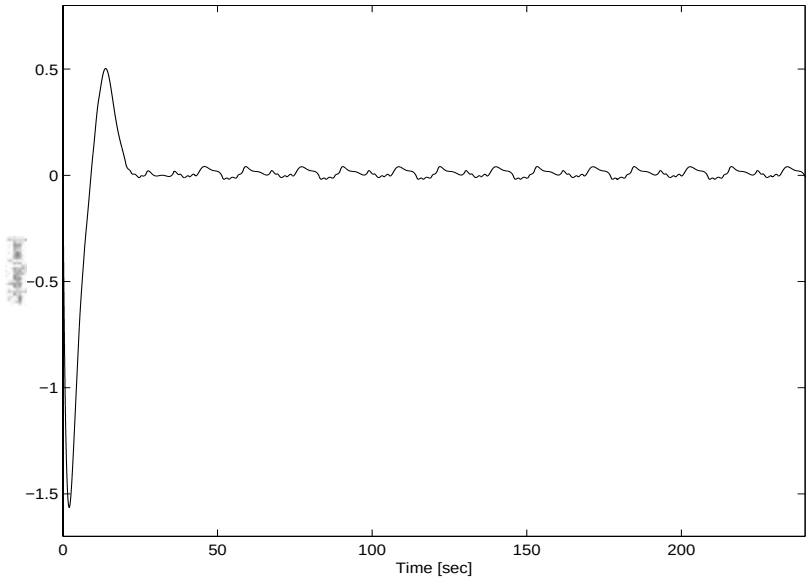

Figure 12: Simulated Angular Velocity Error with Inverted Actuator Nonlinearity

oscillations in the angular velocity error and scaled inertia estimate. The rms value of $\tilde{\omega}$ is about .02 deg/sec and the mean value is 0.01 deg/sec, which is below the noise level of the gyro. The mean value of the scaled inertia estimate is about 40.5 sec with a peak-to-peak amplitude of about .9 sec. Furthermore, simulations show that the scaled inertia estimates converge to the same value for different values of the frequency of $\nu(t)$.

The inverted actuator nonlinearity with the adaptive controller is implemented on the triaxial testbed. The results are shown in Figures 14 to 16. The rms value of $\tilde{\omega}$ is about .15 deg/sec and the mean value is 0.011 deg/sec. The mean value of the scaled inertia is about 39.6 sec and the peak-to-peak amplitude of oscillation is about 2.5 sec. Note that while oscillations in the angular velocity error and inertia estimates are reduced, they are not entirely eliminated. Sensor noise may account for some part of the oscillations seen in Figure 14.

4.4 Real Inertia of the Triaxial Testbed

To determine the actual inertia in kg-m^2/rad^2, test masses are added at known distances from the rotational axis. Let ΔJ, J' and J'' denote the change in inertia, the scaled inertia and the scaled inertia from an experiment with added test masses, respectively. Hence

$$J'' = (J + \Delta J)\frac{K_{\text{gyro}}}{K_{\text{fan}}}, \tag{19}$$

and the inertia in kg-m^2/rad^2 is given by

$$J = \frac{-J'\Delta J}{J' - J''}. \tag{20}$$

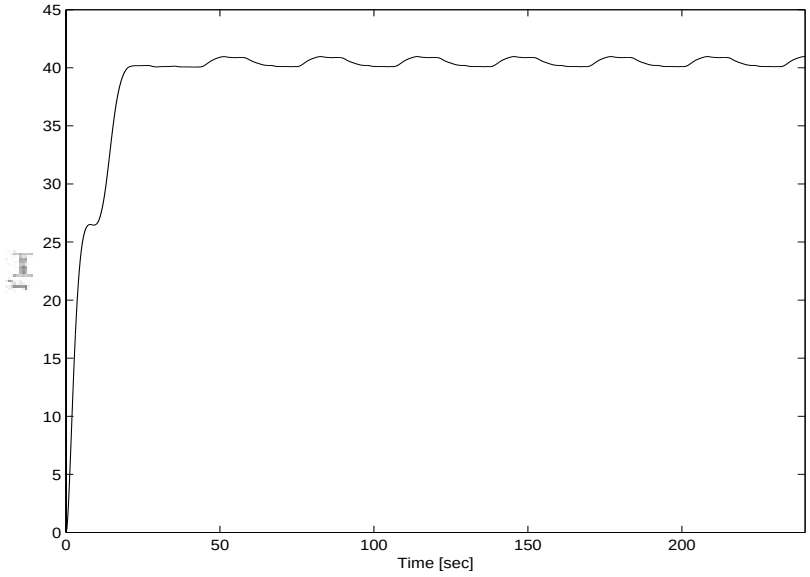

Figure 13: Simulated Scaled Inertia Estimate with Inverted Actuator Nonlinearity

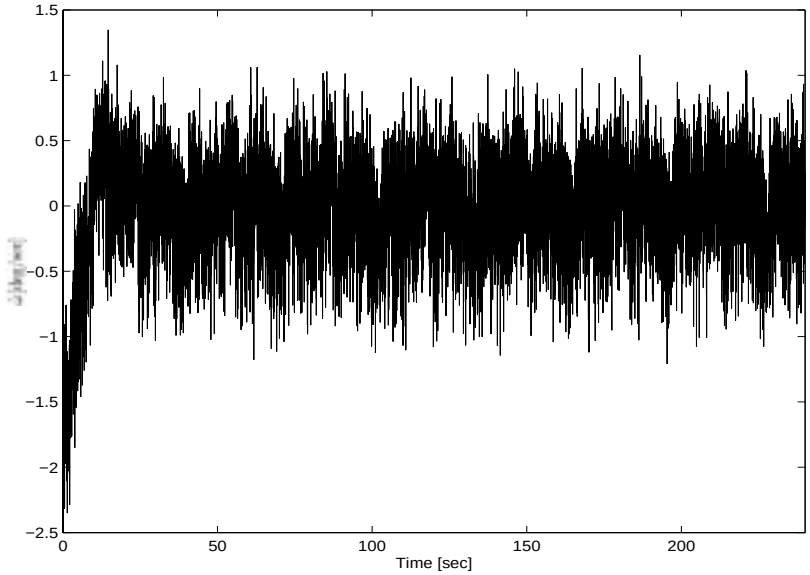

Figure 14: Experimental Angular Velocity Error with Inverted Actuator Nonlinearity

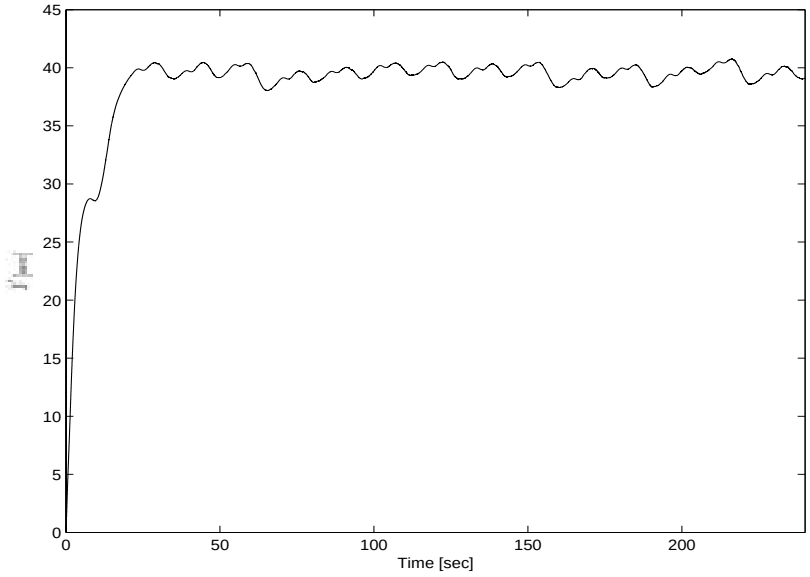

Figure 15: Experimental Scaled Inertia Estimate with Inverted Actuator Nonlinearity

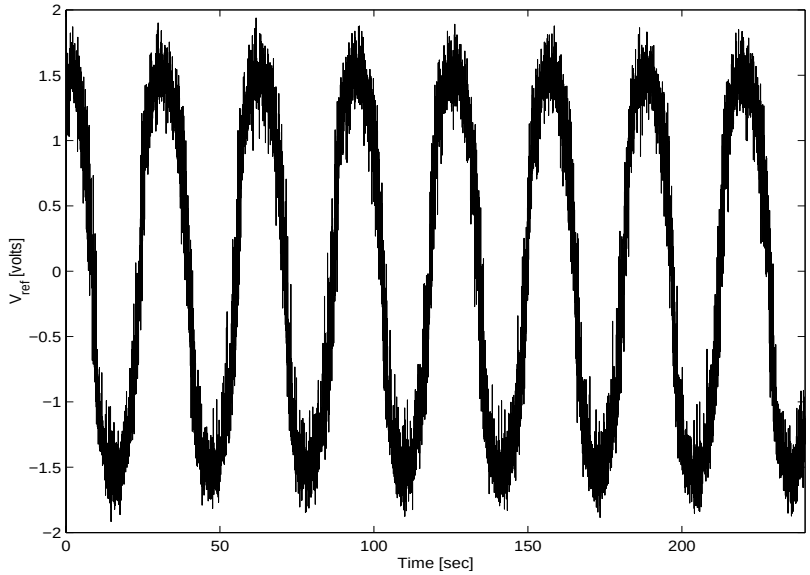

Figure 16: Experimental Control Signal with Inverted Actuator Nonlinearity

A total mass of 5.11 kg is added to the two square mounting plates of the testbed, each at a distance of 0.75 m from the rotational axis. Hence, $\Delta J = 2.87$ kg-m^2/rad^2. Since the scaled inertia estimate $\hat{J}''$ is about 39.6 sec, the real moment of inertia is found to be $J = 66.6$ kg-m^2/rad^2 using equation (20).

5 Approximate Feedback Linearization

5.1 Preliminary Analysis

The single degree of freedom spacecraft dynamics with nonlinear actuation is modeled by

$$\dot{\omega} = \frac{1}{J} h(u), \tag{21}$$

where ω is the spacecraft angular velocity, u is the control signal, J is the moment of inertia, and h: $\mathcal{R} \to \mathcal{R}$ is an unknown one-to-one nonlinear input mapping. With these definitions, the torque applied to the spacecraft axis is $\tau = h(u)$.

Let $\hat{h} : \mathcal{R} \to \mathcal{R}$ be a one-to-one approximation of h with inverse $\hat{h}^{-1}$. For example, $\hat{h}$ may denote the inverted piecewise linear approximation of the cubic nonlinear fit of h as shown in Figure 11. An approximately linearizing feedback control law is then given by

$$u = \hat{h}^{-1}(v), \qquad \text{or} \qquad v = \hat{h}(u). \tag{22}$$

Define $\Delta : \mathcal{R} \to \mathcal{R}$ by

$$\Delta(u) \triangleq h(u) - \hat{h}(u) \tag{23}$$

so that $\Delta(\hat{h}^{-1}(v)) = h(\hat{h}^{-1}(v)) - v$ and $\tau = h(u) = \Delta(u) + v$. Then

$$\dot{\omega} = \frac{1}{J} h(\hat{h}^{-1}(v)) = \frac{1}{J}[v + \Delta(\hat{h}^{-1}(v))]. \tag{24}$$

Now choose $v = v_a - v_c$ so that

$$\dot{\omega} = \frac{1}{J}[v_a + \Delta(\hat{h}^{-1}(v)) - v_c]. \tag{25}$$

Here v_a is the torque specified by the adaptive algorithm (4),(5) for the system (1), and v_c is the torque used to cancel $\Delta(\hat{h}^{-1}(v))$.

5.2 Adaptive Feedback Linearization Control

Assumption 5.1 There exists a known function σ: $\mathcal{R} \to \mathcal{R}^l$ and an unknown vector $M \in \mathcal{R}^l$ such that, for all $v \in \mathcal{R}$,

$$\Delta(\hat{h}^{-1}(v)) = M^{\mathrm{T}} \sigma(v). \tag{26}$$

Using (26), (24) can be written as

$$\dot{\omega} = \frac{1}{J}[v_a + M^{\mathrm{T}}\sigma(v) - v_c]. \tag{27}$$

To approximately cancel $M^{\mathrm{T}}\sigma(v)$ in (25) we use an estimate of $M^{\mathrm{T}}\sigma(v)$ given by $v_c = \hat{M}^{\mathrm{T}}\sigma(v)$, where $\hat{M}$ is an estimate of M. Hence, from (27) we have

$$\dot{\omega} = \frac{1}{J}[v_a + (M - \hat{M})^{\mathrm{T}}\sigma(v)].$$

The vector $\hat{M}$ is updated according to the adaptation law

$$\dot{\hat{M}} = G\tilde{\omega}\sigma(v), \tag{28}$$

where $G \in \mathcal{R}^{l\times l}$ is a positive-definite adaptation gain matrix. Defining the error $\tilde{M} \triangleq \hat{M} - M$, (28) can be written as

$$\dot{\tilde{M}} = G\tilde{\omega}\sigma(v). \tag{29}$$

5.3 Stability Analysis

Theorem 2. Assume that $\nu(t)$ is C^1, $\dot{\nu}$ is bounded, and $\sigma(v)$ is bounded for all $v \in \mathcal{R}$. Let $k > 0$. Consider the system (21), the control (22) and the adaptation law (3), (4) and (28). Then $\tilde{J}$ and $\tilde{M}$ are bounded and $\tilde{\omega} \to 0$ as $t \to \infty$.

Proof. From (25), we have $\dot{\tilde{\omega}} = -\dot{\nu} + \frac{1}{J}[v_a + \Delta(\hat{h}^{-1}(v)) - v_c]$. Since $v_a = -k\tilde{\omega} + \dot{\nu}\hat{J}$ and $\Delta(\hat{h}^{-1}(v)) - v_c = \tilde{M}^T\sigma(v)$, we obtain

$$\dot{\tilde{\omega}} = \frac{1}{J}[-k\tilde{\omega} + \dot{\nu}\tilde{J} - \tilde{M}^T\sigma(v)], \tag{30}$$

$$\dot{\tilde{J}} = -q\dot{\nu}\tilde{\omega}, \tag{31}$$

$$\dot{\tilde{M}} = G\tilde{\omega}\sigma(v), \tag{32}$$

where v is the solution of the equation $v + \hat{M}^T\sigma(v) = -k\tilde{\omega} + \dot{\nu}\hat{J}$.

Next, consider the radially unbounded, positive-definite Lyapunov candidate

$$V(\tilde{\omega}, \tilde{J}, \tilde{M}) = \frac{J}{2}\tilde{\omega}^2 + \frac{1}{2q}\tilde{J}^2 + \frac{1}{2}\tilde{M}^{\mathrm{T}}G^{-1}\tilde{M}. \tag{33}$$

Then along the trajectories of the system,

$$\dot{V}(\tilde{\omega}, \tilde{J}, \tilde{M}) = J\tilde{\omega}\dot{\tilde{\omega}} + \frac{1}{q}\tilde{J}\dot{\tilde{J}} + \tilde{M}^{\mathrm{T}}G^{-1}\dot{\tilde{M}}. \tag{34}$$

Substituting (30), (31) and (32) into (34), we obtain

$$\dot{V}(\tilde{\omega}, \tilde{J}, \tilde{M}) = -k\tilde{\omega}^2 \leq 0.$$

Hence, $V(\tilde{\omega}(t), \tilde{J}(t), \tilde{M}(t)) \leq V(\tilde{\omega}(0), \tilde{J}(0), \tilde{M}(0))$ for all $t \geq 0$. Since V is radially unbounded, it follows that $\tilde{\omega}, \tilde{J}, \tilde{M}$ are bounded.

To show that $\tilde{\omega} \to 0$ as $t \to \infty$, we need only show that $\dot{V}$ is uniformly continuous with respect to time along the state trajectories. To see this, notice that along the state trajectories,

$$\ddot{V}(\tilde{\omega}, \tilde{J}, \tilde{M}) = -\frac{2k}{J}\tilde{\omega}\Big(- k\tilde{\omega} + \dot{\nu}\tilde{J} - \tilde{M}^T\sigma(v)\Big).$$

Since $\tilde{\omega}$, $\tilde{J}$, $\tilde{M}$, $\dot{\nu}$, and $\sigma(v)$ are bounded, $\ddot{V}(\tilde{\omega}(t), \tilde{J}(t), \tilde{M}(t), t)$ is bounded. Hence, $\dot{V}$ is uniformly continuous with respect to time along the state trajectories. Consequently, it follows from Theorem 5.4 of [12] that $\tilde{\omega} \to 0$ as $t \to \infty$. □

The following result presents a method for identifying the inertia J and the coefficients M.

Proposition 3. Consider the system (21). Assume that $k > 0$, $\nu(t)$ is C^1, $\nu(t)$ and $\dot{\nu}(t)$ are bounded, periodic with period T, but not constant, and $\sigma(v)$ is bounded for all $v \in \mathcal{R}$. Let $v(t)$ satisfy $v(t) + \bar{M}^T\sigma(v(t)) = \dot{\nu}(t)\bar{J}$, where $\bar{J} \in \mathcal{R}$ and $\bar{M} \in \mathcal{R}^l$. Furthermore, assume that, for all positive integers k, there exist $l+1$ time instants $t_1, t_2, \ldots, t_{l+1}$ satisfying $kT \leq t_1 < t_2 < \ldots < t_{l+1} \leq (k+1)T$ such that the $(l+1) \times (l+1)$ matrix

$$\begin{bmatrix} \dot{\nu}(t_1) & \dot{\nu}(t_2) & \cdots & \dot{\nu}(t_{l+1}) \\ -\sigma(v(t_1)) & -\sigma(v(t_2)) & \cdots & -\sigma(v(t_{l+1})) \end{bmatrix}$$

is nonsingular for all $\bar{J} \neq 0$ and all $\bar{M} \in \mathcal{R}^l$. Then, under the adaptive control law (3), (4) and (28), $\hat{J} \to J$ and $\hat{M} \to M$ as $t \to \infty$.

Proof. Consider the Lyapunov function V defined by (33) and $\dot{V}$ defined by (34). Let $E \triangleq \dot{V}^{-1}(0) = \{(\tilde{\omega}, \tilde{J}, \tilde{M}) : \tilde{\omega} \equiv 0\}$, and let $\mathcal{M}$ be the largest invariant set in E. Consider a solution $(\tilde{\omega}, \tilde{J}, \tilde{M})$ in $\mathcal{M}$. Since $\tilde{\omega} \equiv 0$, it follows from (31)-(32) that $\dot{\tilde{J}} \equiv 0$ and $\dot{\tilde{M}} \equiv 0$. Therefore, $\tilde{J}, \tilde{M}$, and hence $\hat{J}, \hat{M}$, are constant. Moreover, $\tilde{\omega} \equiv 0$ implies $\dot{\tilde{\omega}} \equiv 0$. By (30), this leads to

$$\dot{\nu}(t)\tilde{J} - \tilde{M}^T\sigma(v(t)) \equiv 0, \tag{35}$$

where $v(t)$ satisfies $v(t) + \bar{M}^T\sigma(v(t)) = \dot{\nu}(t)\bar{J}$, and $\bar{J}, \bar{M}$ are constant.

We now show that $\bar{J}$ cannot be zero. In fact, if $\bar{J} = 0$, then $\tilde{J} = -J \neq 0$ and v satisfies $v + \hat{M}^T\sigma(v) = 0$, which implies that v is constant. Hence, (35) implies $-\dot{\nu}(t)J - \tilde{M}^T\sigma(v) \equiv 0$. Note that $\tilde{M}^T\sigma(v)$ is constant, but $\dot{\nu}(t)J \neq 0$ and is time varying. This leads to a contradiction. Consequently, it is sufficient to consider the case $\bar{J} \neq 0$.

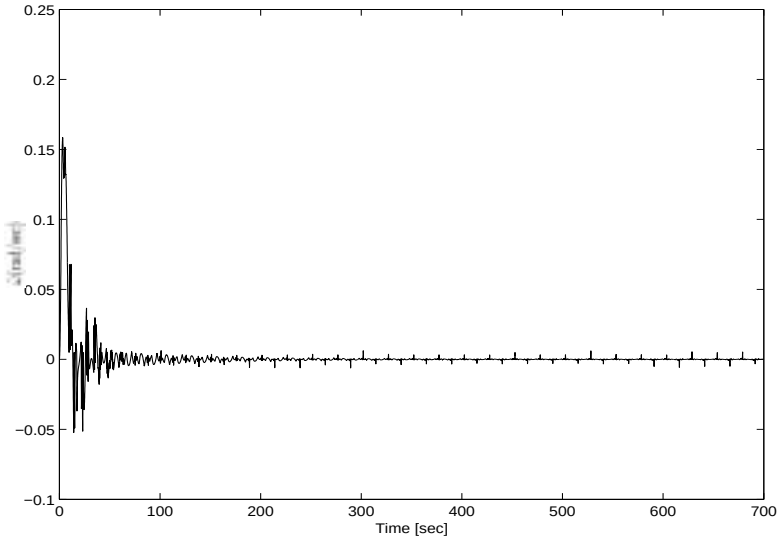

Figure 17: Simulated Angular Velocity Error $\tilde{\omega}$ with Adaptive Feedback Linearization

In any period, we can write (35) at the time instants $t_1, t_2, \ldots, t_{l+1}$ in the matrix form

$$\begin{bmatrix} \tilde{J} & \tilde{M}^T \end{bmatrix} \underbrace{\begin{bmatrix} \dot{\nu}(t_1) & \dot{\nu}(t_2) & \cdots & \dot{\nu}(t_{l+1}) \\ -\sigma(v(t_1)) & -\sigma(v(t_2)) & \cdots & -\sigma(v(t_{l+1})) \end{bmatrix}}_{P} = \begin{bmatrix} 0 & 0 & \cdots & 0 \end{bmatrix}.$$

Since P is nonsingular for all $\bar{J} \neq 0$ and all $\bar{M}$, it follows that $\tilde{J} = 0$ and $\tilde{M} = 0$ as required. □

5.4 Example and Simulation

In this example, we assume $J = 1$ and $h(u) = 0.2u^3$, $\hat{h}(u) = u$ and we choose 11 spline functions for σ. The control signal is selected as $\nu(t) = \sin 0.25t$, and the control parameters in the adaptive control law are

$$k = 1, \quad q = 4.8, \quad G = 80 I_{11\times 11}.$$

The simulation results are shown in Figures 17-18. It is clear that $\tilde{\omega}$ converges to zero and $\tilde{J}$ is bounded as expected. For comparison, we show the angular velocity error $\tilde{\omega}$ and the estimated inertia $\hat{J}$ without the adaptive law in Figures 19 and 20. It can be seen that the adaptive law improves responses of the angular velocity tracking and inertia identification.

6 Conclusions

An adaptive feedback control algorithm has been developed to provide global tracking of commanded spacecraft angular velocity signals. The algorithm assumes no knowledge of the inertia of the spacecraft and is thus unconditionally robust with respect to this parametric uncertainty. It

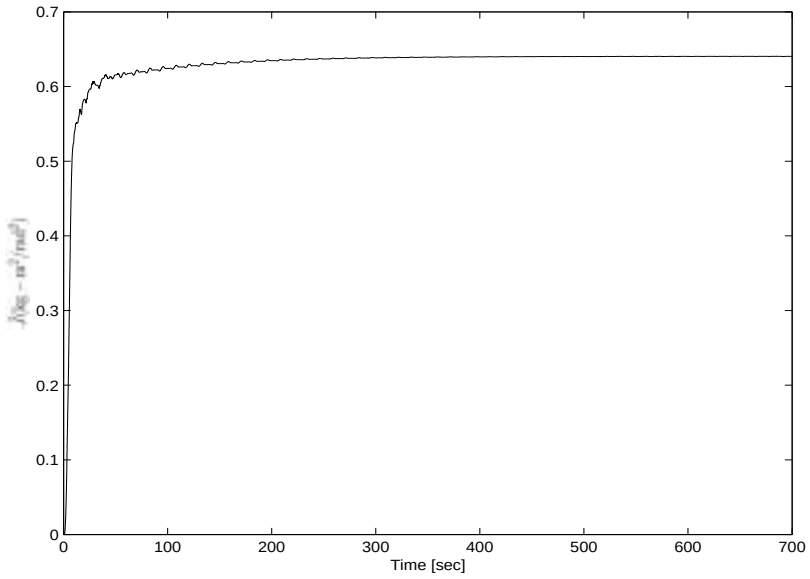

Figure 18: Simulated Estimated Inertia $\hat{J}$ with Adaptive Feedback Linearization

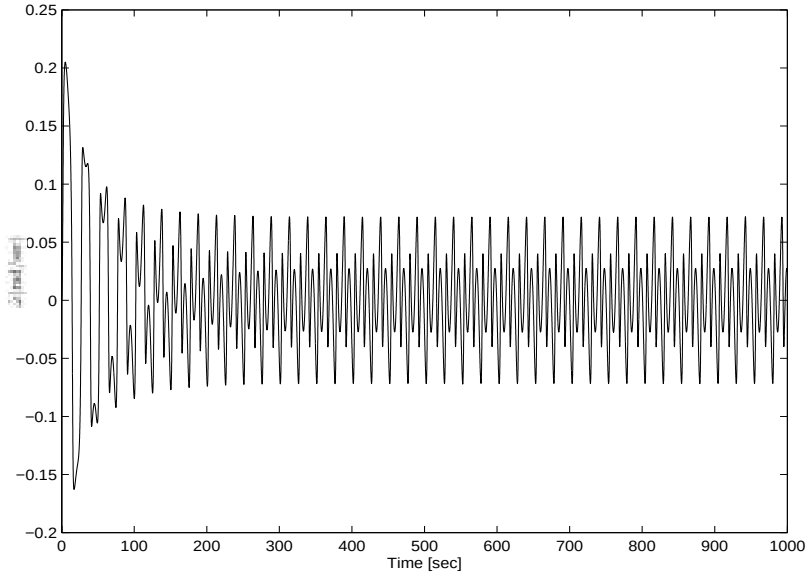

Figure 19: Simulated Angular Velocity Error $\tilde{\omega}$ without Adaptive Feedback Linearization

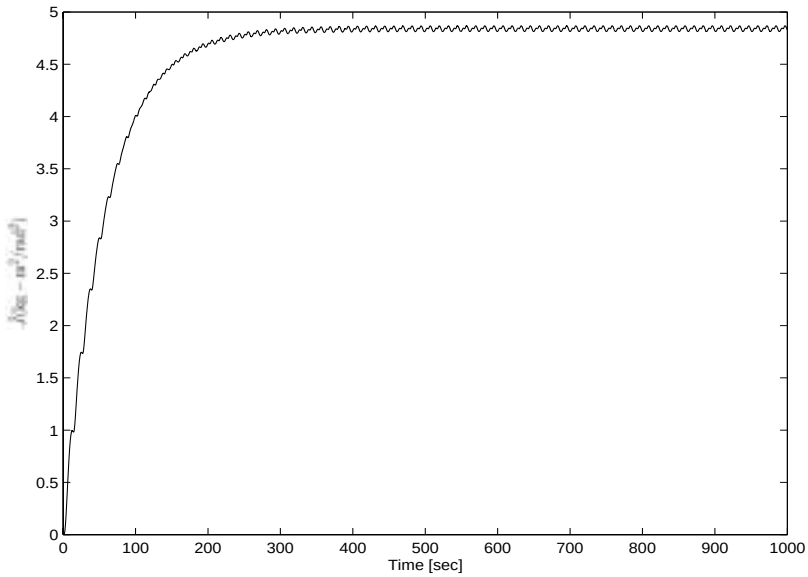

Figure 20: Simulated Estimated Inertia $\hat{J}$ without Adaptive Feedback Linearization

was shown using a Lyapunov argument that the angular velocity tracking error converges to zero. Furthermore, the control algorithm was used to identify the spacecraft inertia matrix when the commanded spacecraft angular velocity signals were continuously differentiable and periodic. Numerical simulations demonstrate tracking and identification of the inertia matrix under such periodic signals.

The one-degree-of-freedom adaptive control algorithm has been implemented on a triaxial attitude control testbed. Experimental results are found to be consistent with simulations. Angular velocity tracking is achieved for constant and sinusoidal signals. Inertia estimates are obtained using the adaptive controller, using sinusoidal commands. An actuator nonlinearity is identified and its effects studied. A piecewise linear approximation of this nonlinearity was inverted and this inverse was found to improve angular velocity tracking by 37.5 percent and inertia identification by 33.3 percent for sinusoidal commands on the testbed.

Finally, an approximate feedback linearization technique was developed, and Lyapunov stability analysis carried out to demonstrate ultimate boundedness of the angular velocity error and inertia estimate error. The focus of current work is in testing and implementation of this technique.

7 Acknowledgements

The last-named author wishes to thank Dr. Naira Hovakimyan for helpful discussions concerning adaptive feedback linearization.

References

[1] R. W. Brockett, "Asymptotic Stability and Feedback Stabilization," in R. W. Brockett, R. S. Millman and H. J. Sussmann, Eds., *Differential Geometric Control Theory*, Progress in Mathematics, Vol. 27, pp. 181-191, 1983.

[2] D. Aeyels and M. Szafranski, "Comments on the Stabilizability of the Angular Velocity of a Rigid Body," *Sys. Contr. Lett.*, Vol. 10, pp. 35-39, 1988.

[3] E. D. Sontag and H. J. Sussmann, "Further Comments on the Stabilizability of the Angular Velocity of a Rigid Body," *Sys. Contr. Lett.*, Vol. 12, pp. 213-217, 1988.

[4] C. I. Byrnes and A. Isidori, "New Results and Examples in Nonlinear Feedback Stabilization," *Sys. Contr. Lett.*, Vol. 12, pp. 437-442, 1989.

[5] C-J. Wan and D. Bernstein, "Nonlinear Feedback Control with Global Stabilization," *Dynamics and Control*, Vol. 5, pp. 321-346, 1995.

[6] R. Outbib and G. Sallet, "Stabilizability of the Angular Velocity of a Rigid Body Revisited," *Sys. Contr. Lett.*, Vol. 18, pp. 93-98, 1992.

[7] J. L. Junkins and J. D. Turner, *Optimal Spacecraft Rotational Maneuvers*, Elsevier Scientific Publishing Company, NY, 1985.

[8] K. D. Bilimoria and B. Wie, "Time-Optimal Three-Axis Reorientation of a Rigid Spacecraft," *J. Guid. Contr. Dyn.*, Vol. 16, No. 3, 1993.

[9] T. A. W. Dwyer, III, and A. L. Batten, "Exact Spacecraft Detumbling and Reorientation Maneuvers with Gimbaled Thrusters and Reaction Wheels," *Astronautical Sci.*, Vol. 33, pp. 217-232, 1985.

[10] J. Dzielski, E. Bergmann, J. Paradiso, D. Rowell and D. Wormley, "Approach to Control Moment Gyroscope Steering Using Feedback Linearization," *J. Guid. Contr.*, Vol. 14, pp. 96-106, 1991.

[11] J. Ahmed, V. T. Coppola and D. S. Bernstein, "Asymptotic Tracking of Spacecraft Attitude Motion with Inertia Matrix Identification," *J. Guid. Contr. Dyn.*, Vol. 21, No. 5, pp. 684-691, 1998

[12] K. J. Astrom and B. Wittenmark, *Adaptive Control*, Addison-Wesley, Reading, MA, 2nd edition, 1995.

[13] K. S. Narendra and A. M. Annaswamy, *Stable Adaptive Systems*, Prentice Hall, Englewood Cliffs, NJ, 1989.

[14] P. A. Ioannou and J. Sun, *Robust Adaptive Control*, Prentice Hall, NJ, 1996.

[15] N. Hovakimyan, F. Nardi, A. Calise, and N. Kim, "Adaptive Output Feedback Control of Uncertain Nonlinear Systems using Single Hidden Layer Neural Networks," *IEEE Trans. Neural Networks*, Vol. 13, pp.1420-1431, 2002.